Published in final edited form as:

Adv Mater Technol. 2020 August ; 5(8): . doi:10.1002/admt.202000325.

A gel-free $Ti_3C_2T_x$-based electrode array for high-density, high-resolution surface electromyography

Brendan B. Murphy,
Department of Bioengineering, 210 S. 33rd Street, 240 Skirkanich Hall, University of Pennsylvania, Philadelphia, PA, United States 19104

Center for Neuroengineering & Therapeutics, 240 S. 33rd Street, 301 Hayden Hall, University of Pennsylvania, Philadelphia, PA, United States 19104

Center for Neurotrauma, Neurodegeneration, and Restoration, 3900 Woodlawn Ave., Corporal Michael J. Crescenz Veterans Affairs Medical Center, Philadelphia, PA, United States 19104

Patrick J. Mulcahey,
Department of Chemistry, 37th & O Streets NW, Georgetown University, Washington, DC, United States 20057

Nicolette Driscoll,
Department of Bioengineering, 210 S. 33rd Street, 240 Skirkanich Hall, University of Pennsylvania, Philadelphia, PA, United States 19104

Center for Neuroengineering & Therapeutics, 240 S. 33rd Street, 301 Hayden Hall, University of Pennsylvania, Philadelphia, PA, United States 19104

Center for Neurotrauma, Neurodegeneration, and Restoration, 3900 Woodlawn Ave., Corporal Michael J. Crescenz Veterans Affairs Medical Center, Philadelphia, PA, United States 19104

Andrew G. Richardson,
Center for Neuroengineering & Therapeutics, 240 S. 33rd Street, 301 Hayden Hall, University of Pennsylvania, Philadelphia, PA, United States 19104

Department of Neurosurgery, 3400 Spruce Street, University of Pennsylvania, Philadelphia, PA, United States 19104

Gregory T. Robbins,
Department of Physical Medicine & Rehabilitation, 1800 Lombard Street, University of Pennsylvania, Philadelphia, PA, United States 19147

Nicholas V. Apollo,
Center for Neuroengineering & Therapeutics, 240 S. 33rd Street, 301 Hayden Hall, University of Pennsylvania, Philadelphia, PA, United States 19104

vitalef@pennmedicine.upenn.edu.

Supporting Information
Supporting Information is available from the Wiley Online Library or from the author.

Conflict of Interest
The authors declare no conflicts of interest.

Center for Neurotrauma, Neurodegeneration, and Restoration, 3900 Woodlawn Ave., Corporal Michael J. Crescenz Veterans Affairs Medical Center, Philadelphia, PA, United States 19104

Kathleen Maleski,
Department of Materials Science and Engineering, A. J. Drexel Nanomaterials Institute, Drexel University, Philadelphia, PA, United States 19104

Timothy H. Lucas,
Center for Neuroengineering & Therapeutics, 240 S. 33rd Street, 301 Hayden Hall, University of Pennsylvania, Philadelphia, PA, United States 19104

Department of Neurosurgery, 3400 Spruce Street, University of Pennsylvania, Philadelphia, PA, United States 19104

Yury Gogotsi,
Department of Materials Science and Engineering, A. J. Drexel Nanomaterials Institute, Drexel University, Philadelphia, PA, United States 19104

Timothy Dillingham,
Department of Physical Medicine & Rehabilitation, 1800 Lombard Street, University of Pennsylvania, Philadelphia, PA, United States 19147

Flavia Vitale
Center for Neuroengineering & Therapeutics, 240 S. 33rd Street, 301 Hayden Hall, University of Pennsylvania, Philadelphia, PA, United States 19104

Center for Neurotrauma, Neurodegeneration, and Restoration, 3900 Woodlawn Ave., Corporal Michael J. Crescenz Veterans Affairs Medical Center, Philadelphia, PA, United States 19104

Department of Physical Medicine & Rehabilitation, 1800 Lombard Street, University of Pennsylvania, Philadelphia, PA, United States 19147

Department of Neurology, 3400 Spruce Street, University of Pennsylvania, Philadelphia, PA, United States 19104

Abstract

Wearable sensors for surface electromyography (EMG) are composed of single- to few-channel large-area contacts, which exhibit high interfacial impedance and require conductive gels or adhesives to record high-fidelity signals. These devices are also limited in their ability to record activation across large muscle groups due to poor spatial coverage. To address these challenges, we have developed a novel high-density EMG array based on titanium carbide ($Ti_3C_2T_x$) MXene encapsulated in parylene-C. $Ti_3C_2T_x$ is a two-dimensional nanomaterial with excellent electrical, electrochemical, and mechanical properties, which forms colloidally stable aqueous dispersions, enabling safe, scalable solutions-processing. Leveraging the excellent combination of metallic conductivity, high pseudocapacitance, and ease of processability of $Ti_3C_2T_x$ MXene, we demonstrate the fabrication of gel-free, high-density EMG arrays which are ~8 μm thick, feature 16 recording channels, and are highly skin-conformable. The impedance of $Ti_3C_2T_x$ electrodes in contact with human skin is 100–1000x lower than the impedance of commercially-available electrodes which require conductive gels to be effective. Furthermore, our arrays can record high-fidelity, low-noise EMG, and can resolve muscle activation with improved spatiotemporal

resolution and sensitivity compared to conventional gelled electrodes. Overall, our results establish $Ti_3C_2T_x$-based bioelectronic interfaces as a powerful platform technology for high-resolution, non-invasive wearable sensing technologies.

Keywords

MXene; electromyography; high-density EMG; wearable sensors; bioelectronics

1. Introduction

1.1. High-Density Surface Electromyography (HDsEMG)

Electromyography (EMG) is a standard procedure used to diagnose a range of neuromuscular pathologies, to investigate motor control disorders, and to study kinesiology and biomechanics.[1–3] EMG can be acquired both invasively and non-invasively, depending on the specific application and required resolution. In surface electromyography (sEMG), the electrical activity generated by skeletal muscles is recorded at the skin surface, in contrast to more invasive intramuscular techniques, which rely on needle electrodes directly inserted into the muscle of interest.[2,3] Typical sEMG involves placing two large-area, metallic contacts over the muscle, recording a bipolar signal, and applying standard filtering techniques to identify global muscle activation following voluntary or evoked muscle contractions. Decomposition algorithms can also be applied to extract additional functional information, such as discharge rates and muscle fiber conduction velocities.[4] In a clinical setting, sEMG is typically adopted to monitor muscle activation and coordination,[5–7] neural control of movement,[8,9] and peripheral nerve/muscle fiber conduction.[10,11] Muscle activation mapping via sEMG is also used for localizing the neuromuscular junction (NMJ), a common target in chemodenervation therapies for muscle spasticity.[12,13]

Mapping the activation and coordination of large muscle groups, as well as accurately localizing the NMJ, requires electrode arrays with large area coverage, and higher channel count.[14] Two-dimensional sEMG arrays —also known as high-density sEMG (HDsEMG) — are well-suited to meet these requirements.[6,15] Typically, HDsEMG arrays are 2D rigid grids of four or more 5–10 mm-diameter contacts, spaced less than 10 mm apart.[14,15] More recently, it has also been shown that electrodes with surface areas < 7 mm^2 should be spaced no more than 10 mm apart in any direction, in order to ensure that the collected sEMG signals are unique and not being aliased.[16] The utility of muscle activation mapping with HDsEMG has been demonstrated in the analysis of single motor units in facial musculature,[17] for localizing the activation area and NMJ in biceps,[18,19] and in approximating motor unit propagation in the *vastus medialis* and *vastus lateralis* during isometric knee extensions.[6,7] Additionally, mm-scale electrodes in high-density montages have been used in clinical settings for tracking motor unit distributions during wrist rehabilitation after stroke,[20] for monitoring motor unit activation in the *biceps brachii* of chronic hemiparetic stroke patients,[21] for amyotrophic lateral sclerosis (ALS) diagnosis and monitoring,[22] and for improving the control of shoulder disarticulation prostheses following targeted muscle reinnervation surgery.[23] However, in most HDsEMG platforms, the millimeter size of the individual electrodes makes maintaining a sufficiently low skin-electrode impedance a significant

challenge. Additionally, achieving high fidelity and high spatial resolution signals from 2D surface recordings is only possible as long as the HDsEMG arrays conform well to the skin surface. These are two critically unmet needs in the landscape of current HDsEMG technologies.

1.2. Materials and Design Strategies for sEMG

Standard electrodes for sEMG recordings are composed of gold (Au), silver (Ag), or silver-silver chloride (Ag/AgCl). Of these, Ag/AgCl electrodes are the most widely used due to their lower baseline noise interface compared to electrodes composed of other metals.[19,24] Most commercially-available Ag/AgCl electrodes are pre-gelled, meaning they feature an electrolytic gel or conductive paste as a coating over the electrode surface. This gel forms the interface between the electrode and the skin during recording, and serves to reduce the interfacial impedance and improve overall signal quality.[24–26] Conductive gels, however, dry out over time, causing skin irritation and significant variations in the interface impedance.[27,28] The gels may also cause other irritating dermatologic reactions, even without drying out, as reported for the gelled electrodes used for vital sign sensing during the Apollo missions to the Moon.[29,30] Furthermore, comparisons between dry and gelled electrodes used for continuous recordings have shown that after 15 min the gelled electrodes are more susceptible to both charge-induced interference, and movement artifacts.[31] Gelled electrodes have also been reported to become more susceptible to movement artifacts as the skin becomes hydrated with sweat or oils from natural perspiration.[32] A high contact impedance between the electrode and the skin results in lower quality sEMG signals, which may adversely affect muscle activation recordings.[33,34] One standard practice to lower the interfacial impedance is to abrade the skin before electrode placement.[25,26,33] This procedure, however, is tedious for the operator and potentially uncomfortable for the subject.

To realize flexible sEMG electrodes with a low interfacial impedance, a variety of materials strategies and device architectures have been proposed. In previous works, very thin layers of metals (usually Au) were deposited onto thin polymeric substrates to serve as electrodes and interconnects, and these ultrathin metallic contacts achieve a relatively low interfacial impedance.[17,34–36] To improve device wearability and skin conformability, sEMG arrays have also been patterned using fractal geometries and microporous structures.[36] As alternatives to metallic contacts, metal nanowires and nanowebs,[37] as well as metal nanoparticles (MNPs),[19,28,38,39] have also been explored. MNP-based HDsEMG arrays have attracted particular attention because they can be fabricated using fast, additive inkjet printing (IJP), which is a high-throughput process with low material waste.[19] Still, the MNP inks must be sintered after deposition, requiring optimization of a thermal treatment process that is compatible with the polymeric substrate material. Since many of the substrates commonly used in wearable electronics have low glass transition temperatures (T_g) — typically, $T_g < 150^{\circ}C$[19,38] — this optimization is non-trivial. Furthermore, once dried, the metallic films resulting from using MNP inks and IJP often have lower surface densities than the same metal films in bulk form,[19] which may result in low electrical conductivity.

Other materials which have been explored for decreasing the contact impedance and improving overall device flexibility include nanostructured carbon allotropes, such as reduced graphene oxide (rGO)[27,40] and carbon nanotubes (CNTs).[41,42] These materials have been readily integrated into electrodes composed of flexible polyester[40] and nylon[27] textile networks, as well as plastic molds.[41,42] However, these configurations require complex, time-consuming fabrication processes to ensure sufficient volume distribution of the conductive carbon filler in the plastic, fabric, or polymeric matrix.[43] Beyond metallic and carbon-based materials, other materials that have been proposed for reducing the skin-electrode impedance include: conductive polymers such as poly(3,4-ethylenedioxythiophene) doped with poly(styrene sulfonate) (PEDOT:PSS) which can be deposited onto the electrode surface,[19] liquid metal inks which can be directly painted onto the skin surface,[44] and ionic liquid gels at the interface between the electrode and the skin which do not dry out at room temperature like most commonly used gels.[45]

While any of the above materials strategies may be beneficial in reducing the skin-electrode interface impedance, there is currently no gel-free HDsEMG technology that readily achieves both a low interfacial impedance, and excellent skin conformability. To address this unmet need, we have developed low-impedance, high-sensitivity, gel-free HDsEMG arrays based on titanium carbide ($Ti_3C_2T_x$) MXene, encapsulated in thin layers of flexible parylene-C. MXenes are a family of two-dimensional early-transition-metal carbides and carbonitrides, of which more than 20 have been synthesized to date, and ~60 have been predicted *in silico*.[46] MXenes are synthesized by selective etching of the A-group element in a ternary-layered MAX phase. MXenes typically contain an abundance of surface terminations (T_x), including hydrophilic oxygen (–O) and hydroxyl (–OH) functional groups, facilitating tunable surface modification. Since MXenes were first synthesized in 2011, they have attracted increasing attention for sensing and electronic applications.[47–51] The most studied and widely used MXene to date is $Ti_3C_2T_x$, which exhibits high electronic conductivity (exceeding ~10,000 S cm^{-1}), has a high optoelectronic figure of merit, and demonstrates remarkable electronic stability under mechanical deformations.[52–54] In the field of biomedicine, $Ti_3C_2T_x$ has been successfully demonstrated as an antibacterial coating,[55] as a photothermal treatment agent in cancer theranostics,[56] and as the primary sensing material in wearable[57,58] and implantable[59,60] bioelectronic platforms. In previous work, we demonstrated a novel fabrication process to integrate $Ti_3C_2T_x$ into microelectrode arrays for recording neural activity *in vivo* in rodent models, and assessed the biocompatibility of MXenes with cultured neuronal cells.[60,61]

Here, we expand the field of $Ti_3C_2T_x$-based bioelectronics to include high-resolution, wearable sensors for HDsEMG recording. Using conventional solution processing and microfabrication techniques, we pattern $Ti_3C_2T_x$ films into thin, highly skin-conformable HDsEMG sensors with remarkably low impedance, without any harsh skin treatment, adhesive, or conductive gel. When compared to commercial, pre-gelled electrodes which are >30x larger in surface area, our $Ti_3C_2T_x$ HDsEMG electrodes exhibit lower impedance, higher sensitivity, and higher signal-to-noise ratio (SNR) in recording sEMG signals. Finally, we demonstrate our $Ti_3C_2T_x$ HDsEMG arrays for applications in neuromuscular cartography, by mapping the spatiotemporal activation of muscles in healthy human subjects with millimeter-scale spatial resolution. The results demonstrated in this work establish, for

the first time, the feasibility of $Ti_3C_2T_x$-based, gel-free epidermal sensors for obtaining high-resolution HDsEMG maps of neuromuscular activation, with significant implications for clinical, rehabilitation, and research applications.

2. Fabrication of $Ti_3C_2T_x$ MXene HDsEMG Arrays

MXenes are easily dispersed in aqueous solutions due to their abundant –O and –OH surface terminations, a property which is unique among nanostructured carbon and other 2D nanomaterials.[52,60] This property is particularly advantageous for fabrication of bioelectronic interfaces, as it enables the use of safe, surfactant-free solution processing methods, which are also compatible with the thermal and chemical requirements of the biocompatible polymeric materials commonly used in such devices.[52,60] In this work, we fabricated $Ti_3C_2T_x$ HDsEMG arrays by integrating spray-casting techniques into a standard microfabrication workflow.[60–62] To precisely pattern $Ti_3C_2T_x$ films into multi-channel HDsEMG contacts, we adopted the sacrificial layer patterning scheme demonstrated in our previous work (Figure 1a–f).[60,61]

A layer of ~4 μm thick parylene-C was deposited via chemical vapor deposition onto a silicon wafer. Metal traces and pads (10nm/100nm Ti/Au) were patterned through standard photolithography, e-beam deposition, and lift-off processes (Figure 1a). Next, the wafer was coated with a dilute Micro90 cleaning solution, to prevent adhesion of subsequent parylene-C layers, followed by a ~3 μm thick sacrificial layer of parylene-C (Figure 1b). HDsEMG contacts overlaying the metal traces were defined in the sacrificial parylene-C layer through photolithography and oxygen plasma reactive ion etching (RIE) (Figure 1c). The wafer was next heated on a hot plate at 150˚C while 300 μL of ~10 mg mL^{-1} $Ti_3C_2T_x$ was spray-coated onto the wafer (Figure 1d). The sacrificial parylene-C layer was then manually peeled up, leaving behind thin $Ti_3C_2T_x$ films only in the patterns that had been defined via RIE (Figure 1e). A final encapsulation layer of ~4 μm of parylene-C was deposited and patterned using photolithography and RIE, and completed devices were peeled off from the wafer for characterization and testing (Figure 1f). Completed arrays consisted of 16-channel grids (4 × 4) of 1.6 mm × 1.6 mm $Ti_3C_2T_x$ square electrodes, encapsulated in a ~8 μm thick layer of parylene-C. Interelectrode distances were 4 mm in the vertical plane and 5.5 mm in the horizontal plane. The flexibility of completed arrays, as well as their excellent conformability to the curved contours of the skin, are illustrated in the panels of Figure 1h. Using a similar fabrication process without the MXene deposition and patterning steps, Au HDsEMG arrays were also fabricated, to allow for a direct comparison of the impedance and recording properties between Au and $Ti_3C_2T_x$.

3. Results and Discussion

3.1. Impedance measurements in saline and on human skin

As an initial characterization of the $Ti_3C_2T_x$ device performance, we performed electrochemical impedance spectroscopy (EIS) in the frequency range of 1–10^5 Hz, in a standard three-electrode cell in phosphate buffered saline (PBS, Quality Biological, pH 7.4). We used a 3 mm diameter nonaqueous Ag/AgCl electrode (CH Instruments) as the reference electrode, and a 1 cm diameter graphite rod as the counter electrode. We compared a single

$Ti_3C_2T_x$ HDsEMG array (n = 16 working channels) to an Au device with the same geometry and dimensions. Figure S1 in Supporting Information shows the impedances of the $Ti_3C_2T_x$ and Au arrays across the frequency spectrum. At 1 kHz, the impedance values were 301 ± 56 Ω and 399 ± 38 Ω for $Ti_3C_2T_x$ and Au, respectively. The U.S. Food and Drug Administration (FDA) guidelines on performance parameters for wearable electrodes[63,64] indicate that the 10 Hz impedance is the primary reference value. Accordingly, at 10 Hz the $Ti_3C_2T_x$ and Au HDsEMG arrays had average impedance moduli of 0.46 ± 0.16 kΩ and 20 ± 3.4 kΩ, respectively. Thus, in the relevant frequency regime for sEMG recording, the $Ti_3C_2T_x$ array shows a >40x reduction in absolute impedance compared to size-matched Au electrodes.

Following EIS in saline, we also measured the impedance at the skin-electrode interface, which is one of the main factors affecting the quality of sEMG recordings.[15,24] To determine the optimal skin-preparation conditions for impedance assays, we first measured the cutaneous impedance[19,45] of our $Ti_3C_2T_x$ electrodes under different skin treatments. The skin of a single healthy subject's forearm was cleaned with an alcohol preparation pad, and three different treatments were tested: (1) no further treatment, (2) abrading the skin with 3M TracePrep abrasive tape, and (3) applying drops of PBS to the skin surface and immediately placing the $Ti_3C_2T_x$ array. The Experimental Section of this report, and Figure S2 (Supporting Information), summarize this preliminary skin treatment assessment. We found that application of PBS and immediate placement of the $Ti_3C_2T_x$ array resulted in sufficiently low skin impedances, and thus, the gel-free $Ti_3C_2T_x$ HDsEMG arrays do not necessarily require abrasive or irritating skin treatments in order to achieve comparably low cutaneous impedances for acute recording. This will likely help to minimize patient discomfort during sEMG recording sessions.

We next sought to compare the cutaneous impedance of the $Ti_3C_2T_x$ electrodes to size-matched Au, and to ~1 cm diameter commercial pre-gelled electrodes (019–439400 Disposable Disc Adhesive Electrodes, Natus Medical Inc.). Accordingly, we placed the $Ti_3C_2T_x$ array along the subject's forearm, following the PBS skin preparation described above, and two additional Natus electrodes were placed as the reference and counter electrodes at the wrist and elbow of the subject's same arm, respectively. We then acquired EIS in the $1–10^5$ Hz range. Then, we replaced the $Ti_3C_2T_x$ array with an Au array on the same subject and repeated the study. Finally, we replaced the Au array with 6 separate Natus electrodes in the same region of the forearm, and repeated the cutaneous impedance measurements for these commercial gelled electrodes. Figure 2a,b shows the Bode plots of the skin-electrode impedance moduli and phase.

As expected, the cutaneous impedances for the HDsEMG arrays were higher than those measured in saline solution: the 1 kHz impedance for $Ti_3C_2T_x$ and Au were 7.1 ± 2.4 kΩ and 7.3 ± 5.0 kΩ respectively—nearly 25x larger than the impedances of the same electrodes in saline. This significant increase in impedance reflects the highly complex nature of the electrode-skin interface: physiological factors like sweat and the various layers of subcutaneous fat attenuate electrical signals that reach the skin surface, adding a highly complex "biological impedance" component to the overall circuit. This biological impedance can vary drastically depending on the individual subject, as well as the ambient

conditions during recording.[24,65] Nevertheless, at 1 kHz the impedances of the HDsEMG arrays were comparable to the pre-gelled Natus electrodes (6.2 ± 1.1 kΩ). Furthermore, at lower frequencies ($f < 100$ Hz), in the regime more relevant to sEMG recording, the $Ti_3C_2T_x$ contacts showed significantly reduced interfacial impedances relative to not only the size-matched Au electrodes, but also compared to the 31x larger Natus electrodes (Figure 2a).

Given that the skin treatment under each of the electrode types was identical, the differences in impedance behavior must be attributed to the electrode materials and sizes, rather than to variability in skin condition. To highlight these contributions, we compared the 10 Hz cutaneous impedance modulus, normalized by the electrode geometric surface area (GSA), of the $Ti_3C_2T_x$ and Au HDsEMG arrays to that of other clinically relevant electrodes (Figure 2c). Specifically, we compared to: Natus pre-gelled electrodes (0.8 cm^2), Covidien H124SG EMG pre-gelled electrodes (3.14 cm^2), 3M's Red Dot™ adhesive patches (10.1 cm^2), and ConMed Cleartrace® 1700-O30 pre-gelled contacts (5.1 cm^2). The GSA of the $Ti_3C_2T_x$ and Au HDsEMG contacts was 0.0256 cm^2. The average GSA-normalized skin impedance of the dry $Ti_3C_2T_x$ electrodes was 0.55 kΩ cm^2, which is ~5x lower than size-matched Au contacts (2.9 kΩ cm^2), and >100x lower than the larger clinical contacts from Natus (169 kΩ cm^2), Covidien (4.3×10^3 kΩ cm^2), 3M (490 kΩ cm^2), and ConMed (570 kΩ cm^2). The significantly improved skin-electrode impedance of the $Ti_3C_2T_x$ HDsEMG arrays over Au and many clinical standards can be attributed to the mechanical properties of the device, which enables high skin-conformability, as well as to the superior electrochemical behavior and high effective surface area of the $Ti_3C_2T_x$ MXene films.[60] Furthermore, it has been well-documented in the literature that $Ti_3C_2T_x$ films can exhibit high pseudocapacitance,[66] with volumetric capacitances up to 900 F cm^{-3} in certain electrolytes, and up to 1500 F cm^{-3} when fabricated into hydrogel film electrodes.[67] $Ti_3C_2T_x$ also exhibits a high gravimetric capacitance, up to 140 F g^{-1} in alkaline electrolytes.[68] To investigate the potential benefit of $Ti_3C_2T_x$ MXene's enhanced capacitive behavior when in contact with human skin, we fitted the impedance spectra with the equivalent circuit modeling of the skin-electrode impedance (Figure S3 and Table S1, Supporting Information).[69,70] The results highlight that $Ti_3C_2T_x$ MXene exhibits higher double-layer capacitance (C_{dl}) on the skin compared to pre-gelled Ag/AgCl and Au: $Ti_3C_2T_x$ shows C_{dl} of 1.57 ± 0.58 μF cm^{-2} ($\chi^2 = (6.24 \pm 1.39)\times10^{-3}$), which is ~2x greater than the C_{dl} of the Au contacts (724.32 ± 192.40 nF cm^{-2}; $\chi^2 = (2.34 \pm 0.40)\times10^{-2}$) and ~20x greater than the C_{dl} of the Natus contacts (69.52 ± 16.18 nF cm^{-2}; $\chi^2 = (8.03 \pm 1.15)\times10^{-3}$). It is worth noting that we measured such superior impedance behavior of the $Ti_3C_2T_x$ arrays without the use of conductive gels or adhesives, which are critically required to achieve suitable skin-electrode impedances in all pre-packaged clinical electrodes.

3.2. Baseline sEMG Recording

To assess whether the low skin impedance of the $Ti_3C_2T_x$ arrays translates into higher fidelity recordings of muscle activity, we next conducted a series of experiments to acquire HDsEMG from the muscles of healthy human subjects. For these tests, four adult subjects (1 male, 3 females, avg. age = 25 ± 2 yrs.) were recruited and consented following an approved protocol from the Institutional Review Board at the University of Pennsylvania. Subjects had

no prior history of neuromuscular disorder, neuropathy, or myopathy, according to self-report.

In healthy subjects, muscle activation may be either evoked through electrical stimulation[10,24] or may occur naturally through voluntary contraction and relaxation of a given muscle group.[2,15,24] To validate our $Ti_3C_2T_x$ arrays for high-resolution sEMG recording, we first demonstrated their utility at resolving voluntary muscle activation. Following skin cleaning with an alcohol prep pad and application of the PBS skin treatment, the $Ti_3C_2T_x$ arrays were placed onto the forearms of three of the four subjects, above the *flexor digitorum superficialis* (FDS) (Figure 3a). Pre-gelled Natus leads were placed as a reference on the wrist, and as a ground electrode on the elbow, of each subject's same arm containing the array. Each subject was then asked to complete at least five voluntary contraction tasks, in the form of making a fist, holding it, and then relaxing. Each task lasted for 5 s, with 10 s of rest in between. During this time, HDsEMG was continuously recorded using a 128-channel Intan Stimulation/Recording Controller, at a sampling rate of 20 kHz. Following recording with the $Ti_3C_2T_x$ array, the same test was repeated using an Au array and a single Natus contact placed in the same location as the $Ti_3C_2T_x$ array. Data was notch-filtered offline at 60 Hz, followed by bandpass filtering between 85–400 Hz.[36,71] The root-mean-square (RMS) envelope of the filtered signal was then calculated using a 200 ms wide moving window, with 25 ms of overlap.[19,36] Representative recordings from one subject, for each type of electrode, are shown in Figure 3c.

To quantify the recording performance, we computed the SNR for each type of electrode. An epoch was defined as the 5 s of contraction ± 3 s (Figure 3e). Within each epoch, signal was defined as the maximum of the RMS envelope during the maximum voluntary contraction (MVC Regime),[72] while noise was defined as the average RMS in the 3 s preceding the contraction (Baseline Regime). The SNR in each epoch was then calculated as the ratio of these two values, and the epochal SNRs were averaged. For the $Ti_3C_2T_x$ and Au arrays, the average SNR for the entire recording session was computed by summing over the SNRs for each epoch, at each of the 16 channels individually, and then averaging across the total number of epochs. The following equation was used:

$$SNR_{tot} \quad [\text{in dB}] = \frac{1}{N}\sum_{n=1}^{N}\sum_{i=1}^{16}\left(snr_n^i\right) \quad , \tag{1}$$

where N is the number of voluntary contraction epochs considered in the analysis, and

$$snr_n^i = 20 \times \log_{10}\left(\frac{\max(RMS_{MVC}) \quad \text{on electrode } i \text{ in epoch } n}{\text{mean}(RMS_{Baseline}) \quad \text{on electrode } i \text{ in epoch } n}\right). \tag{2}$$

For one subject, the $Ti_3C_2T_x$ HDsEMG array had an average SNR of 39 ± 16 dB over ten completed contractions, which is higher than the SNRs of both the size-matched Au electrodes (13 ± 7 dB), and the larger-area Natus contact (9 ± 5 dB) during the same number of completed contractions for that same subject. The $Ti_3C_2T_x$ arrays for the other subjects also showed higher SNRs compared to Au and Natus, and the results are summarized in Table S2 (Supporting Information). Next, looking at the power spectral density of the raw

sEMG during the voluntary contraction tasks, we found more power in the signal recorded on the $Ti_3C_2T_x$ contacts than on either Au or Natus electrodes (Figure 3d). This was true across the entire frequency spectrum, but specifically in the region of particular interest for sEMG recording, suggesting that $Ti_3C_2T_x$ is more sensitive for recording voluntary muscle activation than either Au or pre-gelled Ag/AgCl.

3.3. High-Resolution Mapping of Muscle Activation

Highly sensitive surface electrodes could significantly improve diagnostic accuracy in muscle cartography studies, where the spatiotemporal propagation of activation is tracked across the muscle during voluntary movement or evoked responses. The ability to map spatiotemporal patterns of muscle activation at high resolution can be valuable in gait and fatigue studies,[9,11] rehabilitation and physical therapy strategies,[8] and myoelectric prosthesis control.[73–75] It may also better inform denervation procedures for reducing muscle tone and spasticity.[12,13] To demonstrate the functionality of the $Ti_3C_2T_x$ HDsEMG arrays for muscular cartography studies, we tracked muscle activation during voluntary force exertion tasks for all four of the recruited subjects. In these experiments, the skin over each subject's *thenar eminence* (TE) muscle group was cleaned with an alcohol prep pad, the PBS skin treatment was applied, and then the recording electrodes—either HDsEMG arrays of Au or $Ti_3C_2T_x$, or a single Natus electrode—were removed from their initial place over the subject's FDS, and were repositioned over the subject's TE for subsequent recordings. A reference electrode was placed on the first metacarpal bone of each subject's thumb, and a ground electrode was placed on the back of each subject's hand. Subjects were next asked to hold a load cell between their thumb and index finger, and to subsequently pinch the load cell at different force levels while their sEMG was recorded (Figure 4a). Since the load cell was pre-loaded, force exertions were recorded as negative deflections from the pre-loaded baseline (Figure 4b). The action of pinching the load cell is an example of opposition between the thumb and index finger, resulting in activation of the *abductor pollicis brevis* (APB) and *opponens pollicis* (OP) muscle branches of the TE muscle group.[76,77] This activity is the sEMG signal that was recorded with the $Ti_3C_2T_x$, Au, or Natus electrodes.

In general, contraction forces and sEMG signal intensity are known to be linearly correlated, following the equation

$$\log(EMG) = k \cdot \log(F), \tag{3}$$

where EMG represents the rectified and smoothed sEMG signal over the length of the contraction, and F is the instantaneous value of the force.[78] Thus, the slope of the line, k, is a measure of the electrode sensitivity. Correlating the maximum exerted force in a given epoch versus the sEMG intensity at that force value for each of the different types of electrodes across all subjects (Figure S4 and Table S3, Supporting Information), we found that the $Ti_3C_2T_x$ electrodes ($k = 50\ mV_{RMS}\ N^{-1}\ cm^{-2}$) were ~10x more sensitive than the Au electrodes ($k = 5\ mV_{RMS}\ N^{-1}\ cm^{-2}$), and ~50x more sensitive than Natus electrodes ($k = 2\ mV_{RMS}\ N^{-1}\ cm^{-2}$) for resolving changing force levels. This result confirms the findings of our SNR analysis, showing that $Ti_3C_2T_x$ endows epidermal electrodes with higher sensitivity than either Au or pre-gelled Ag/AgCl.

Next, we mapped changes in the RMS envelope of the HDsEMG signal collected with the $Ti_3C_2T_x$ arrays, and observed a distinct spatiotemporal evolution of the underlying muscle activity during each force exertion epoch. Figure 4b–f shows representative data from one epoch of opposition between the thumb and forefinger, from one subject. During the pinch grip phase of this particular task (F = 0.3 N, 11% of F_{max} = 2.4 N, Figure 4c), muscle activation initially emerged under channels 7 and 8 of the array. At 56% of F_{max} (~1.3 N), the APB branch of the TE group began to activate, as evidenced by higher amplitudes and a larger zone of activation in the area around channels 7 and 8 (Figure 4d). The maximum force exertion corresponded to the highest activation in APB, occurring still beneath channels 7 and 8. There was also a further widening of the active muscle zone, seen in the preferential spreading of activity along the left side of the array (Figure 4e). This spread likely indicates the recruitment of the OP branch of the TE group, following increased pinching force on the load cell. During the relaxation phase of this task (Figure 4f), we saw clear deactivation of the TE group, spreading from APB in the bottom-center, to OP along the left side of the array. The preferential activation of only a portion of the mapped region, and the relative invariance of the RMS response of the channels in the upper-right corner of the array during the entire loading epoch, suggest that this part of the array was over top of a region not as highly involved in the action of pinching the load cell. Anatomically, the *flexor pollicis brevis* (FPB) is another muscle branch belonging to the TE muscle group, which is not as implicated in opposition of the thumb and index finger as are APB and OP.[76,77] Therefore, it is reasonable to conclude that the upper-right corner of the $Ti_3C_2T_x$ array was laying over FPB.

Altogether, the data demonstrates that the $Ti_3C_2T_x$ HDsEMG arrays can be used for highly sensitive, highly specific muscle cartography. Due to the high density and small sizes of the electrodes in the HDsEMG array, we can precisely discriminate between areas of muscle activity, even in a small muscle group such as the TE, with millimeter-scale resolution. Current single, large-area sEMG contacts are too coarse to localize the region of muscle activity at this resolution, and they also cannot clearly resolve spatiotemporal patterns of recruitment and deactivation among individual muscles in a group.

4. Conclusion

In the present study, we developed a high-density, gel-free electrode array for sEMG based on $Ti_3C_2T_x$ MXene encapsulated in flexible parylene-C. The combination of high conductivity, hydrophilic surface terminations, and good mechanical flexibility from $Ti_3C_2T_x$ MXene, as well as the thinness and conformability of the parylene-C encapsulation, resulted in a significantly lower skin-electrode impedance, removing the need for conductive gels or excessive skin treatments to help lower the impedance. sEMG recorded using the $Ti_3C_2T_x$ arrays during voluntary contraction and force exertion tasks showed higher SNRs and sensitivity compared to size-matched Au electrodes and larger clinical gelled electrodes. High-density, high-resolution mapping of muscle activation in the *thenar eminence* muscle group during varying levels of exerted force allowed for the clear identification of distinct regions of activation, and enabled tracking of the spatiotemporal patterns of recruitment and deactivation at the millimeter scale. This work establishes, for the first time, the many benefits of high-density sEMG recording as enabled by wearable, low impedance $Ti_3C_2T_x$

MXene bioelectronic interfaces. This novel technology has a number of potential applications in electrodiagnostics, rehabilitation, assistive technologies, and basic science studies into the fundamental mechanisms underlying neuromuscular function and disease. Furthermore, the advantages of these conformable, gel-free wearable sensors could have a transformative impact on a number of other skin-based bioelectronic applications, including non-invasive brain, cardiac, and electrodermal response monitoring.

5. Experimental Section

$Ti_3C_2T_x$ HDsEMG Array Fabrication:

a 4” silicon wafer was coated with ~4 μm of parylene-C. Metal traces and pads (10nm/100nm Titanium/Gold) were patterned using standard photolithography, electron-beam evaporation, and lift-off processes. The wafer was coated with an anti-adhesive layer (2% Micro90 cleaning solution) and then a second layer of sacrificial parylene-C, ~3 μm in thickness, was deposited. $Ti_3C_2T_x$ electrode contacts and traces were defined by photolithography using the negative photoresist NR71–3000p, and the sacrificial parylene-C layer was etched using oxygen plasma reactive ion etching (RIE). The wafer was placed on a hot plate pre-set to 150 ˚C, and then 300 μL of a solution of $Ti_3C_2T_x$ MXene dispersed in deionized water to a concentration of ~10 mg mL^{-1} was spray-coated onto the wafer using a commercial airbrush (Gocheer) connected to a TC-20 air compressor unit. $Ti_3C_2T_x$ films made via spray-coating were ~200 nm thick, as determined by mechanical profilometry. After spray-coating, the wafer was baked at 150 ˚C for 15 min in air, to ensure that the resulting $Ti_3C_2T_x$ thin film was fully dried. A 75 nm layer of SiO_2 was deposited via electron-beam evaporation to serve as a protective coating for the $Ti_3C_2T_x$ films during later fabrication steps. The sacrificial parylene-C layer was removed manually with tweezers, leaving behind SiO_2-coated $Ti_3C_2T_x$ thin films only in the patterns defined by the RIE etch step. A ~4 μm thick parylene-C layer was deposited as the final encapsulation layer, and then an etch mask was defined via photolithography. 100 nm of aluminum (Al) was deposited via electron-beam evaporation and lift-off was performed, resulting in the outline of the final devices and openings over the Ti/Au bonding pads and the $Ti_3C_2T_x$ electrode contacts. Using oxygen plasma RIE, the exposed parylene-C on the wafer was etched away. Next, the Al etch mask was removed by wet etching in Al Etchant Type A (Transene). The SiO_2 protective layer over the $Ti_3C_2T_x$ contacts was etched away with a 1:6 buffered oxide etchant (BOE: 6 parts 40% NH_4F, 1 part 49% HF, Sigma Aldrich), exposing the $Ti_3C_2T_x$ electrodes. A similar procedure was used to fabricate the Au HDsEMG arrays, except that Au was deposited via electron-beam evaporation in place of the step where $Ti_3C_2T_x$ is spray-coated onto the wafer. Completed devices were removed from the silicon wafer manually with tweezers, with the aid of drops of deionized water applied near the device edges. Devices were inserted into zero-insertion force (ZIF) connectors soldered onto custom printed circuit boards, for interfacing with the data acquisition systems for electrochemical impedance spectroscopy (EIS) and sEMG recordings.

Impedance Spectroscopy:

EIS *in vitro*, as well as on the skin (cutaneous EIS), was performed using a Gamry Reference 600 Potentiostat/Galvanostat/ZRA, along with the associated software (Gamry

Framework, v7.8). For *in vitro* EIS, a 10 mM PBS (pH 7.4) at room temperature was used as the supporting electrolyte. For cutaneous EIS, human skin was the supporting medium. All EIS measurements were collected using a three-electrode configuration. For *in vitro* EIS, the $Ti_3C_2T_x$ or Au HDsEMG arrays were the working electrode, a graphite carbon rod (1 cm diameter, Bio-Rad Laboratories, Inc.) was the counter electrode, and a nonaqueous Ag/AgCl electrode (3 mm diameter, CH Instruments, Inc.) was the reference electrode. For cutaneous EIS, the $Ti_3C_2T_x$ or Au HDsEMG arrays, or individual pre-gelled Ag/AgCl electrodes from Natus® (019–439400 Disposable Disc Adhesive Electrodes, ~1 cm diameter) were the working electrode, and the pre-gelled Natus electrodes were used for both the counter and reference electrodes. For all EIS measurements, a 10 mV (peak-to-peak amplitude) sinusoidal signal was applied, and the frequency was swept from 1 to 10^5 Hz.

Testing the Effects of Skin Treatment on Skin Impedance:

a single healthy human subject was recruited, and the skin of both of their forearms was cleaned with a sterile alcohol preparation pad (70% IPA, Fisherbrand™). The skin of one forearm was abraded with 3M TracePrep tape and a single $Ti_3C_2T_x$ HDsEMG array was attached to the skin surface. On the other forearm, drops of PBS were applied to the skin surface before a separate $Ti_3C_2T_x$ HDsEMG array was immediately placed. The cutaneous impedance was collected at 8 channels of the two $Ti_3C_2T_x$ HDsEMG arrays on either arm, using a three-electrode configuration with pre-gelled Natus contacts placed as the reference and counter electrodes at the wrists and elbows of the subject's arms, respectively. A Gamry Reference 600 potentiostat was used for the impedance measurements (see Impedance Spectroscopy Section above). After recording the skin impedance under these two skin treatments, the arrays were removed, and the skin was recleaned on one of the subject's forearms with an alcohol prep pad. Then, one of the $Ti_3C_2T_x$ HDsEMG arrays was replaced on the skin and the cutaneous impedance from 8 channels was collected for this no treatment control. Figure S2 in Supporting Information shows the Bode plot of the impedance modulus for each of the skin treatments explored in this preliminary study.

sEMG Recordings:

sEMG signals were recorded in order to evaluate the performance of the $Ti_3C_2T_x$ HDsEMG arrays relative Au HDsEMG arrays and monopolar Ag/AgCl contacts from Natus. Recording electrodes were placed over either FDS or TE, depending on the experimental protocol, and pre-gelled Natus electrodes were used as the reference and ground electrodes for all sEMG recordings. When the recording electrodes were placed over the FDS, the reference electrode was placed at the subject's wrist, and the ground electrode was placed at the subject's elbow. When recording from the TE, the reference electrode was placed on the head of the first metacarpal bone of the thumb, and the ground electrode was placed on the back of the subject's hand. All sEMG signals were acquired at 20 kS/s, using a 128-channel amplifier (Intan RHS2000 Stimulation/Recording Controller, Intan Technologies). Force exertion data was acquired using a pre-loaded load cell (Omega Engineering, Inc.) connected to one of the Analog-In ports of the same recording amplifier. All sEMG recording procedures were approved by the Institutional Review Board at the University of Pennsylvania.

sEMG Analysis:

all signal processing (filtering), data display, and calculations on recorded sEMG or load cell data were completed using custom scripts written in Matlab®. For all sEMG recordings, a 60 Hz notch filter was applied to remove line noise. Power spectral density (PSD) analysis was completed on this notch-filtered data. After PSD analysis, a bandpass filter was applied from 85–400 Hz,[36] and for comparison purposes across electrode types and between the channels of the HDsEMG arrays, an RMS envelope was calculated from the filtered sEMG recordings using Matlab's built-in *rms()* function and a moving window with a width of 200 ms and an overlap of 25 ms SNR calculations were completed based on the RMS envelopes. Activation maps were also generated from the RMS envelopes, to demonstrate the HDsEMG array ability to spatiotemporally track muscle activation. Force exertion levels recorded with the load cell were unfiltered.

Supplementary Material

Refer to Web version on PubMed Central for supplementary material.

Acknowledgements

This manuscript was written through contributions of all authors. All authors have given approval to the final version of the manuscript. This work was supported by: the Mirowski Family Foundation and Neil and Barbara Smit (F.V.); the NIH training Fellowship in Neuroengineering and Medicine (grant no. T32NS091006 to N.V.A.); and the National Science Foundation Graduate Research Fellowship Program (grant no. DGE-1845298 to N.D. and B.B.M.). MXene development at Drexel University was supported by Murata Manufacturing Co., Ltd. This work was performed in part at the University of Pennsylvania's Singh Center for Nanotechnology, an NNCI member supported by NSF Grant ECCS-154253. Any opinions, findings, and conclusions or recommendations expressed in this material are those of the authors, and do not reflect the views of the National Institutes of Health, Department of Veterans Affairs, or the National Science Foundation.

References

[1]. Wu Y, Martínez MÁ, Balaguer PO, in Electrodiagnosis New Front. Clin. Res (Eds: Martínez MÁ, Turker H), IntechOpen, Rijeka, Croatia, 2013.

[2]. Merletti R, Rainoldi A, Farina D, Exerc. Sport Sci. Rev 2001, 29, 20. [PubMed: 11210442]

[3]. Hug F, J. Electromyogr. Kinesiol 2011, 21, 1. [PubMed: 20869882]

[4]. Reaz MBI, Hussain MS, Biol. Proced. Online 2006, 8, 11. [PubMed: 16799694]

[5]. Drost G, Stegeman DF, van Engelen BGM, Zwarts MJ, J. Electromyogr. Kinesiol 2006, 16, 586. [PubMed: 17085302]

[6]. Martinez-Valdes E, Laine CM, Falla D, Mayer F, Farina D, Clin. Neurophysiol 2016, 127, 2534. [PubMed: 26778718]

[7]. Martinez-Valdes E, Negro F, Laine CM, Falla D, Mayer F, Farina D, J. Physiol 2017, 595, 1479. [PubMed: 28032343]

[8]. Vigotsky AD, Halperin I, Lehman GJ, Trajano GS, Vieira TM, Front. Physiol 2018, 8, 985. [PubMed: 29354060]

[9]. Tao W, Liu T, Zheng R, Feng H, Sensors (Basel) 2012, 12, 2255. [PubMed: 22438763]

[10]. Farina D, Blanchietti A, Pozzo M, Merletti R, Neuromuscolare S, Elettronica D, Torino P, Blanchietti A, Pozzo M, J. Appl. Physiol 2019, 97, 545.

[11]. Troiano A, Naddeo F, Sosso E, Camarota G, Merletti R, Mesin L, Gait Posture 2008, 28, 179. [PubMed: 18490165]

[12]. Chang E, Ghosh N, Yanni D, Lee S, Alexandru D, Mozaffar T, Crit. Rev. Phys. Rehabil. Med 2013, 25, 11. [PubMed: 25750484]

[13]. Simon O, Yelnik AP, Eur. J. Phys. Rehabil. Med 2010, 46, 401. [PubMed: 20927006]
[14]. Farina D, Negro F, Gazzoni M, Enoka RM, J. Neurophysiol 2008, 100, 1223. [PubMed: 18497352]
[15]. Merletti R, Holobar A, Farina D, J. Electromyogr. Kinesiol 2008, 18, 879. [PubMed: 19004645]
[16]. Afsharipour B, Soedirdjo S, Merletti R, Biomed. Signal Process. Control 2019, 49, 298.
[17]. Lapatki BG, van Dijk JP, Jonas IE, Zwarts MJ, Stegeman DF, J. Appl. Physiol 2004, 96, 327. [PubMed: 12972436]
[18]. Rasool G, Afsharipour B, Suresh NL, Rymer WZ, IEEE Trans. Neural Syst. Rehabil. Eng 2017, 25, 1802. [PubMed: 28320672]
[19]. Roberts T, De Graaf JB, Nicol C, Hervé T, Fiocchi M, Sanaur S, Adv. Healthc. Mater 2016, 5, 1462. [PubMed: 27125475]
[20]. Potočnik B, Divjak M, Urh F, Member S, in IEEE Trans. Neural Syst. Rehabil. Eng, 2020, p. 99.
[21]. Kallenberg LAC, Hermens HJ, Muscle Nerve 2009, 39, 177. [PubMed: 19034958]
[22]. Bashford J, Mills K, Shaw C, Clin. Neurophysiol 2020, 131, 942. [PubMed: 32044239]
[23]. Zhou P, Lowery MM, Dewald JPA, Kuiken TA, in 2005 IEEE Eng. Med. Biol. 27th Annu. Conf, IEEE, 2005, pp. 4064–4067.
[24]. Merletti R, Botter A, Troiano A, Merlo E, Minetto MA, Clin. Biomech 2009, 24, 122.
[25]. Cattarello P, Merletti R, in 2016 IEEE Int. Symp. Med. Meas. Appl. MeMeA 2016 - Proc, Benevento, Italy, 2016.
[26]. Piervirgili G, Petracca F, Merletti R, Physiol. Meas 2014, 35, 2101. [PubMed: 25243492]
[27]. Yapici MK, Alkhidir T, Samad YA, Liao K, Sensors Actuators, B Chem. 2015, 221, 1469.
[28]. Scalisi RG, Paleari M, Favetto A, Stoppa M, Ariano P, Pandolfi P, Chiolerio A, Org. Electron. Physics, Mater. Appl 2015, 18, 89.
[29]. Ochia RS, Cavanagh PR, J. Electromyogr. Kinesiol 2007, 17, 365. [PubMed: 16723259]
[30]. Johnston RS, Dietlein LF, Berry CA, Biomedical Results of APOLLO, 1975.
[31]. Searle A, Kirkup L, Physiol. Meas 2000, 271. [PubMed: 10847194]
[32]. Pylatiuk C, Müller-Riederer M, Kargov A, Schulz S, Schill O, Reischl M, Bretthauer G, in 2009 IEEE 11th Int. Conf. Rehabil. Robot, 2009, pp. 300–304.
[33]. Hewson DJ, Langeron Y, Duche J, J. Electromyogr. Kinesiol 2003, 13, 273. [PubMed: 12706606]
[34]. Yamagami M, Peters KM, Milovanovic I, Kuang I, Yang Z, Lu N, Steele KM, Sensors (Basel) 2018, 18, 1269.
[35]. Nawrocki RA, Jin H, Lee S, Yokota T, Sekino M, Someya T, Adv. Funct. Mater 2018, 28, 678.
[36]. Tian L, Zimmerman B, Akhtar A, Yu KJ, Moore M, Wu J, Larsen RJ, Lee JW, Li J, Liu Y, Metzger B, Qu S, Guo X, Mathewson KE, Fan JA, Cornman J, Fatina M, Xie Z, Ma Y, Zhang J, Zhang Y, Dolcos F, Fabiani M, Gratton G, Bretl T, Hargrove LJ, V Braun P, Huang Y, Rogers JA, Nat. Biomed. Eng 2019, 3, 194. [PubMed: 30948811]
[37]. Lee E, Kim I, Liu H, Cho G, Fibers Polym 2017, 18, 1749.
[38]. Matsuhisa N, Kaltenbrunner M, Yokota T, Jinno H, Kuribara K, Sekitani T, Someya T, Nat. Commun 2015, 6, 7461. [PubMed: 26109453]
[39]. Khan Y, Pavinatto FJ, Lin MC, Liao A, Swisher SL, Mann K, Subramanian V, Maharbiz MM, Arias AC, Adv. Funct. Mater 2016, 26, 1004.
[40]. Lou C, Li R, Li Z, Liang T, Wei Z, Run M, Yan X, Liu X, Sensors (Basel) 2016, 16, 1833.
[41]. Jung H, Moon J, Baek D, Lee J, Choi Y, Hong J, IEEE Trans. Biomed. Eng 2012, 59, 1472. [PubMed: 22410324]
[42]. Kim JH, Hwang JY, Hwang HR, Kim HS, Lee JH, Seo JW, Shin US, Lee SH, Sci. Rep 2018, 8, 1375. [PubMed: 29358581]
[43]. Yao S, Swetha P, Zhu Y, Adv. Healthc. Mater 2018, 7, 1700889.
[44]. Yu Y, Zhang J, Liu J, PLoS One 2013, 8, 8.
[45]. Leleux P, Johnson C, Strakosas X, Rivnay J, Hervé T, Owens RM, Malliaras GG, Adv. Healthc. Mater 2014, 3, 1377. [PubMed: 24591460]

[46]. Anasori B, Gogotsi Y, 2D Metal Carbides and Nitrides (MXenes), Springer Nature Switzerland AG, Cham, Switzerland, 2019.

[47]. Zhang Y, Lee KH, Anjum DH, Sougrat R, Jiang Q, Kim H, Alshareef HN, Sci. Adv 2018, 4, eaat0098. [PubMed: 29922718]

[48]. Zhang J, Wan L, Gao Y, Fang X, Lu T, Pan L, Xuan F, Adv. Electron. Mater 2019, 5, 1900285.

[49]. An H, Habib T, Shah S, Gao H, Radovic M, Sci. Adv 2018, 4, eaaq0118. [PubMed: 29536044]

[50]. Tan H, Tao Q, Pande I, Majumdar S, Liu F, Persson POÅ, Rosen J, Van Dijken S, Zhou Y, Nat. Commun 2020, 11, 1369. [PubMed: 32170075]

[51]. Lei Y, Zhao W, Zhang Y, Jiang Q, He J, Baeumner AJ, Wolfbeis OS, Wang ZL, Salama KN, Alshareef HN, Small 2019, 15, 1901190.

[52]. Dillon AD, Ghidiu MJ, Krick AL, Griggs J, May SJ, Gogotsi Y, Barsoum MW, Fafarman AT, Adv. Funct. Mater 2016, 26, 4162.

[53]. Maleski K, Ren CE, Zhao MQ, Anasori B, Gogotsi Y, ACS Appl. Mater. Interfaces 2018, 10, 24491. [PubMed: 29956920]

[54]. Hantanasirisakul K, Zhao M, Urbankowski P, Halim J, Anasori B, Kota S, Ren CE, Barsoum MW, Gogotsi Y, Adv. Electron. Mater 2016, 2, 1600050.

[55]. Rasool K, Mahmoud KA, Johnson DJ, Helal M, Berdiyorov GR, Gogotsi Y, Sci. Rep 2017, 7, 1598. [PubMed: 28487521]

[56]. Liu G, Zou J, Tang Q, Yang X, Zhang Y, Zhang Q, Huang W, Chen P, Shao J, Dong X, ACS Appl. Mater. Interfaces 2017, 9, 40077. [PubMed: 29099168]

[57]. Lin H, Chen Y, Shi J, Adv. Sci 2018, 5, 1800518.

[58]. Huang K, Li Z, Lin J, Han G, Huang P, Chem. Soc. Rev 2018, 47, 5109. [PubMed: 29667670]

[59]. Xu B, Zhu M, Zhang W, Zhen X, Pei Z, Xue Q, Zhi C, Shi P, Adv. Mater 2016, 28, 3333. [PubMed: 26924616]

[60]. Driscoll N, Richardson AG, Maleski K, Anasori B, Adewole O, Lelyukh P, Escobedo L, Cullen DK, Lucas TH, Gogotsi Y, Vitale F, ACS Nano 2018, 12, 10419. [PubMed: 30207690]

[61]. Driscoll N, Maleski K, Richardson AG, Murphy B, Anasori B, Lucas TH, Gogotsi Y, Vitale F, J. Vis. Exp 2020, 15, e60741.

[62]. Sessolo M, Khodagholy D, Rivnay J, Maddalena F, Gleyzes M, Steidl E, Buisson B, Malliaras GG, Adv. Mater 2013, 25, 2135. [PubMed: 23417987]

[63]. FDA-2019-D-1649: Cutaneous Electrodes for Recording Purposes – Performance Criteria for Safety and Performance Based Pathway, 2019.

[64]. ANSI/AAMI EC12 — Disposable ECG Electrodes, 2000.

[65]. Li G, Wang S, Duan YY, Sensors Actuators, B Chem. 2017, 241, 1244.

[66]. Ando Y, Okubo M, Yamada A, Otani M, Adv. Funct. Mater 2020, 2000820.

[67]. Xiong D, Li X, Bai Z, Lu S, Small 2018, 14, 1703419.

[68]. Xu S, Wei G, Li J, Ji Y, Klyui N, Izotov V, Han W, Chem. Eng. J 2017, 317, 1026.

[69]. Beckmann L, Neuhaus C, Medrano G, Jungbecker N, Walter M, Gries T, Leonhardt S, 1, Physiol. Meas 2010, 31, 233. [PubMed: 20086274]

[70]. Heikenfeld J, Jajack A, Rogers J, Gutruf P, Tian L, Pan T, Li R, Lab Chip 2017, 18, 217.

[71]. De Luca CJ, Gilmore LD, Kuznetsov M, Roy SH, J. Biomech 2010, 43, 1573. [PubMed: 20206934]

[72]. Wiedemann LG, Mcdaid AJ, IEEE Life Sci. Conf 2017, 137.

[73]. Sudarasan S, Sekaran DEC, Procedia Eng. 2012, 38, 3547.

[74]. Khushaba RN, Kodagoda S, Takruri M, Dissanayake G, Expert Syst. Appl 2012, 39, 10731.

[75]. Radmand A, Scheme E, Englehart K, J. Rehabil. Res. Dev 2016, 53, 443. [PubMed: 27532260]

[76]. Napier JR, J. Anat 1951, 86, 335.

[77]. Kozin SH, Porter S, Clark P, Diego S, Thoder JJ, J. Hand Surg. Am 1999, 24A, 64.

[78]. Perry Jacquelin, Bekey GA, Crit. Rev. Biomed. Eng 1981, 7, 1. [PubMed: 7042199]

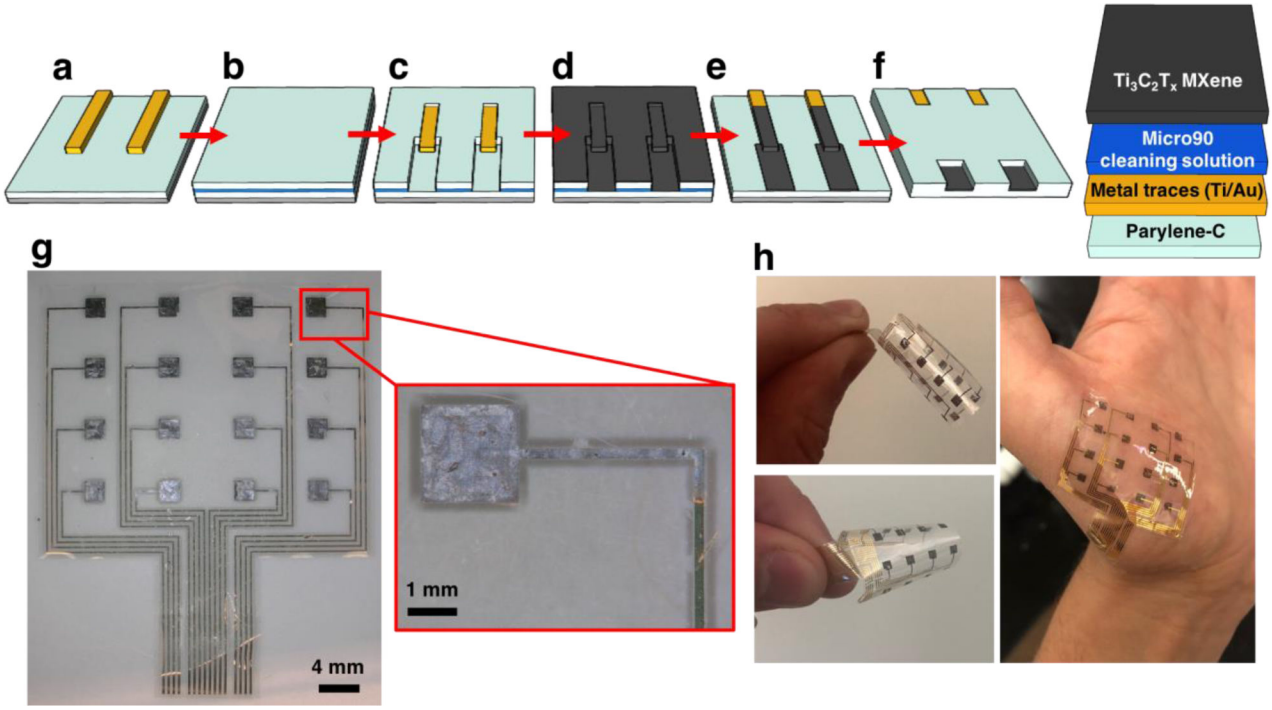

Figure 1.

Fabrication of multi-channel $Ti_3C_2T_x$ HDsEMG arrays. **a)** Deposition of bottom-layer parylene-C, followed by patterning and lift-off of the Ti/Au metal traces; **b)** deposition of the anti-adhesive (Micro90 cleaning solution) and sacrificial parylene-C layers; **c)** reactive ion etching to pattern the sacrificial parylene-C layer; **d)** spray-coating of $Ti_3C_2T_x$ MXene onto the wafer; **e)** "dry lift-off" of the sacrificial parylene-C layer; **f)** top-layer parylene-C encapsulation, patterning of the electrode and bonding pad openings, and release of completed devices from the substrate. **g)** Light microscopy image of a completed 16-channel $Ti_3C_2T_x$ HDsEMG array, with a higher magnification image of a single $Ti_3C_2T_x$ contact. **h)** Demonstration of the flexibility and skin conformability of completed $Ti_3C_2T_x$ HDsEMG arrays.

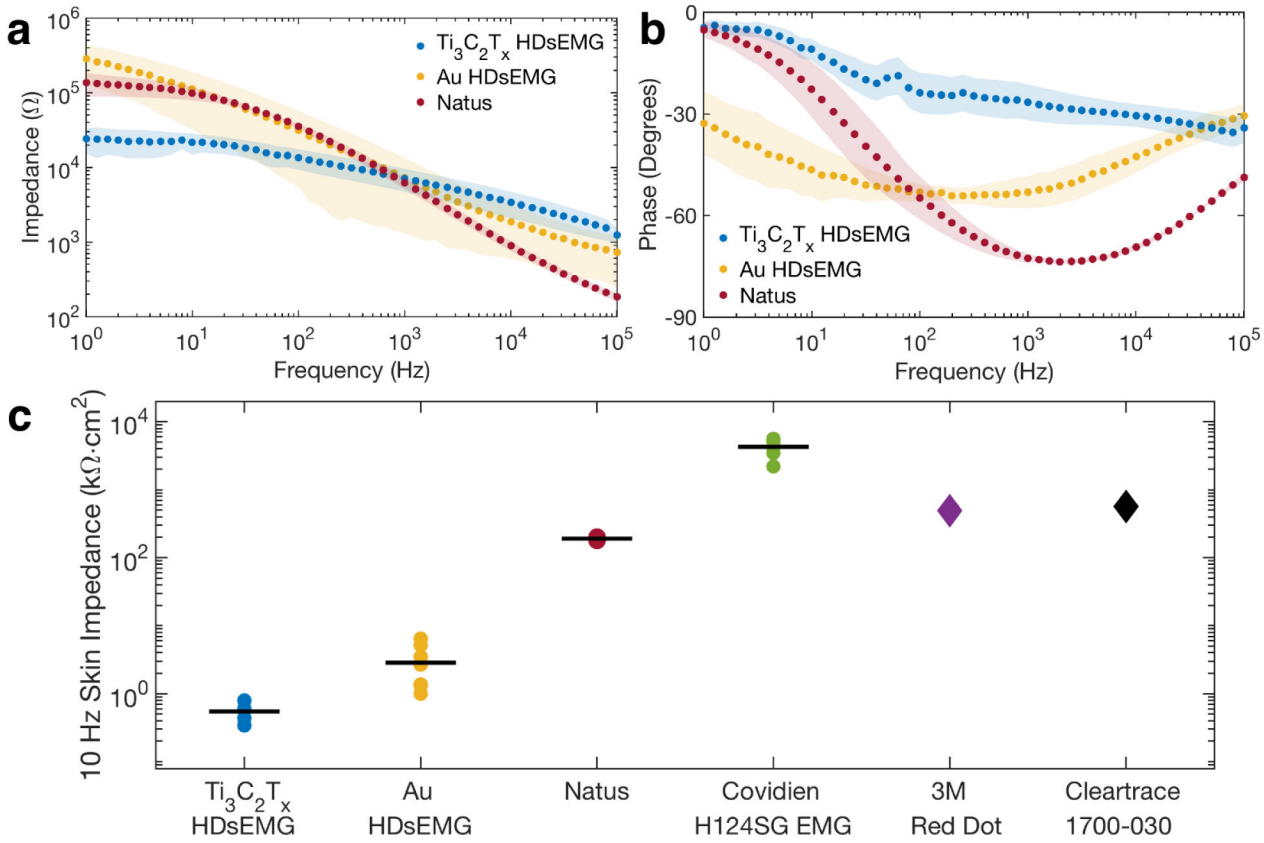

Figure 2.

Electrochemical impedance of the skin-electrode interface. **a)** Bode plot of the cutaneous impedance modulus for $Ti_3C_2T_x$ and Au HDsEMG arrays compared with Natus pre-gelled Ag/AgCl disk electrodes. The skin treatment beneath all of the electrode types was the same (the PBS skin treatment). Data points represent means, shaded regions show standard deviations. $n_{Ti3C2Tx} = n_{Au} = 16$ contacts, and $n_{Natus} = 6$ contacts. **b)** Bode plot of the cutaneous impedance phase for the same electrodes as in (a). **c)** Scatter plot of the area-normalized 10 Hz impedance moduli for (from left to right): 16-channel $Ti_3C_2T_x$ and Au HDsEMG arrays, Natus disposable disk electrodes, Covidien H124SG EMG pre-gelled Ag/AgCl electrodes, 3M Red Dot™ adhesive patches, and ConMed Cleartrace® 1700-O30 commercial electrodes. Data points represent individual channels for the HDsEMG arrays (n = 8 channels for each array). For Natus and Covidien, points represent individual electrodes (n = 6 separate contacts). Solid black lines denote means. Values for the 3M and Cleartrace contacts were obtained from product datasheets.

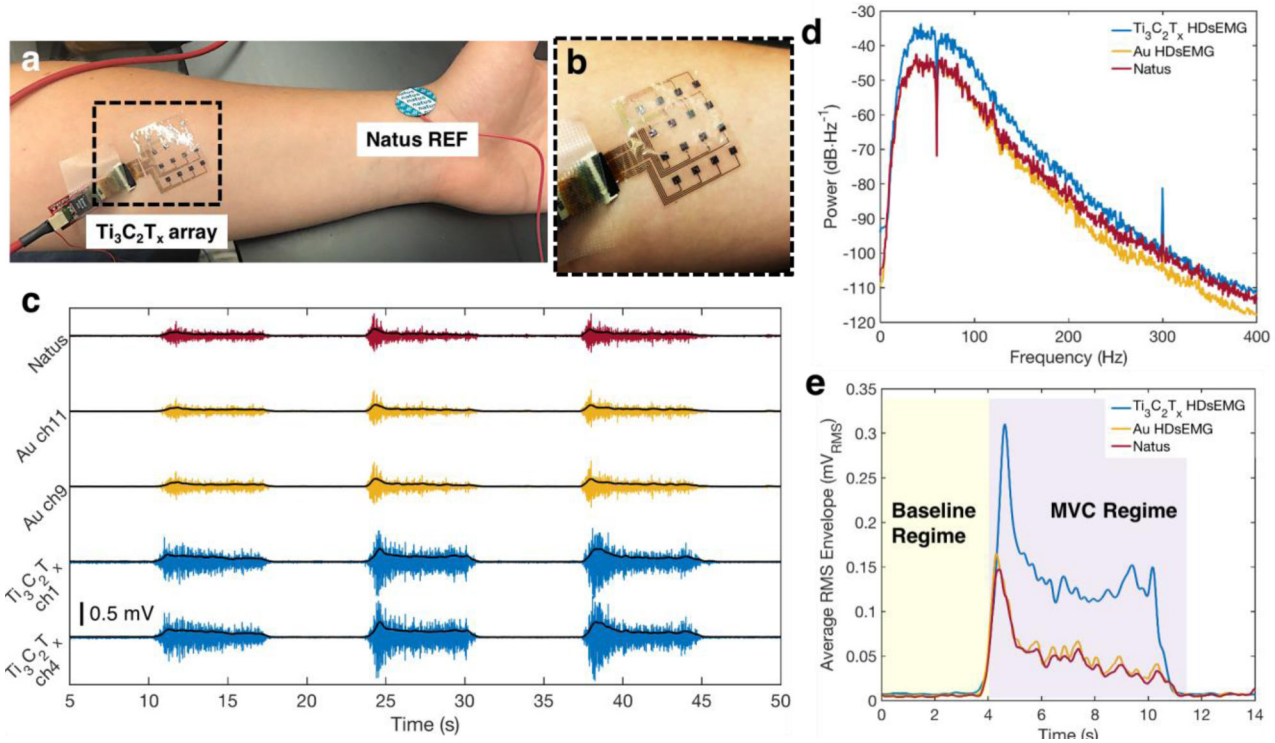

Figure 3.

Baseline sEMG recordings with the $Ti_3C_2T_x$ and HDsEMG arrays, and a Natus monopolar contact. **a)** Experimental setup for a standard voluntary contraction recording experiment. The $Ti_3C_2T_x$ array is placed over the *flexor digitorum superficialis*, while Natus electrodes are placed on the elbow (not shown) and at the wrist, as ground and reference, respectively. **b)** Close-up image of the $Ti_3C_2T_x$ array, showing its excellent skin conformability. **c)** Examples of the sEMG signal recorded from the FDS during a typical voluntary contraction experiment on two channels from the $Ti_3C_2T_x$ and Au HDsEMG arrays, and a single Natus contact, for one subject. The RMS envelope of the sEMG signal is overlaid in black for each trace. Signals were recorded separately for the $Ti_3C_2T_x$ array and the Au and Natus electrodes, but data was time- and amplitude-matched offline, for ease of viewing. **d)** Average power spectral density of the baseline sEMG recordings on all channels of the $Ti_3C_2T_x$ and Au arrays, and a single Natus contact, for one subject. Note that a 60 Hz notch filter was applied to the data for all contacts. **e)** The average RMS envelope of the sEMG signal during the first contractions shown in (c), comparing the magnitudes of the RMS signals recorded on each of the three electrode types. A value was computed for the SNR for each electrode, using RMS values in the Baseline and MVC Regimes shaded in yellow and purple, respectively.

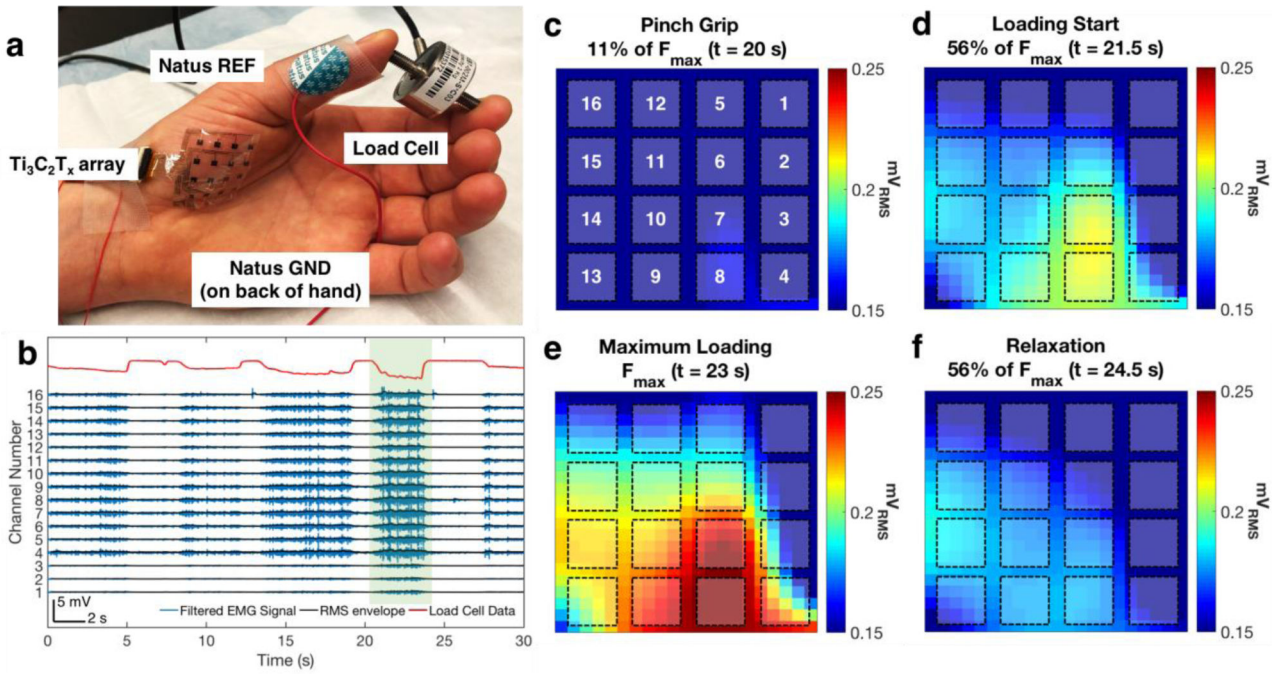

Figure 4.

High-resolution mapping of muscle activation with the $Ti_3C_2T_x$ HDsEMG array. **a)** Picture of the experimental setup. The $Ti_3C_2T_x$ array is placed over the *thenar eminence* muscle group of the thumb, and the subject is asked to pinch a load cell between the thumb and forefinger at varying levels of exerted force. Reference and ground electrodes (Natus monopolar contacts) are placed on the head of the first metacarpal bone, and on the back of the hand, respectively. **b)** Example of HDsEMG and force data recorded during a load cell experiment. The top trace, in red, is the force intensity recorded at the load cell, while the traces in blue are the recorded sEMG for each channel in the $Ti_3C_2T_x$ array. Approximately 5 loading epochs are shown in this recording. RMS envelopes are overlaid on the sEMG data, shown in black. **c–f**) RMS maps generated during the epoch highlighted in green in (b). RMS maps were generated during the **c)** pinch grip, **d)** loading start, **e)** maximum loading, and **f)** relaxation phases of the task. Locations of the channels of the $Ti_3C_2T_x$ array are overlaid on top of the RMS maps, with the channel numbering shown in (c).